JOURNAL OF MATERIALS SCIENCE 27 (1992) 2141–2147

Processing maps for hot-working of powder metallurgy 1100 Al–10 vol % SiC–particulate metal-matrix composite

B. V. RADHAKRISHNA BHAT, Y. R. MAHAJAN
Defence Metallurgical Research Laboratory, Hyderabad 500 258, India

H. MD. ROSHAN
Department of Metallurgical Engineering, Indian Institute of Technology, Madras 600 036, India

Y. V. R. K. PRASAD
Department of Metallurgy, Indian Institute of Science, Bangalore 560 012, India

The hot-working characteristics of the metal-matrix composite (MMC) Al–10 vol % SiC-particulate (SiC_p) powder metallurgy compacts in as-sintered and in hot-extruded conditions were studied using hot compression testing. On the basis of the stress–strain data as a function of temperature and strain rate, processing maps depicting the variation in the efficiency of power dissipation, given by $\eta = 2m/(m + 1)$, where m is the strain rate sensitivity of flow stress, have been established and are interpreted on the basis of the dynamic materials model. The as-sintered MMC exhibited a domain of dynamic recrystallization (DRX) with a peak efficiency of about 30% at a temperature of about 500 °C and a strain rate of 0.01 s^{-1}. At temperatures below 350 °C and in the strain rate range 0.001–0.01 s^{-1} the MMC exhibited dynamic recovery. The as-sintered MMC was extruded at 500 °C using a ram speed of 3 mm s^{-1} and an extrusion ratio of 10 : 1. A processing map was established on the extruded product, and this map showed that the DRX domain had shifted to lower temperature (450 °C) and higher strain rate (1 s^{-1}). The optimum temperature and strain rate combination for powder metallurgy billet conditioning are 500 °C and 0.01 s^{-1}, and the secondary metal-working on the extruded product may be done at a higher strain rate of 1 s^{-1} and a lower temperature of 425 °C.

1. Introduction

MMCs based on aluminium reinforced with SiC_p were first reported by Divecha *et al.* [1] and the various aspects of their properties were reviewed by Nair *et al.* [2]. In addition to the attractive properties common to all composites, such as high specific stiffness, high specific strength, high-temperature resistance and improved wear resistance, these MMCs possess the additional advantage of amenability to secondary metal-working processes, unlike composites with continuous fibre reinforcement. However, the formability of MMCs is greatly restricted by the incompatible deformation characteristics of the soft matrix and the hard reinforcement. The optimum processing parameters for the matrix material do not hold good for the composite, and the general method of optimizing the process parameters by trial-and-error methods would prove uneconomical. Recently, the use of processing maps for the optimization of processing parameters has been found to be very useful [3]. Tuler and Klimowicz [4] developed processing maps for alumina–aluminium alloy-cast MMCs and validated them using successful forging trials.

The aim of the present investigation was to study the constitutive flow behaviour of aluminium reinforced with SiC_p MMC under hot-working conditions and to generate a processing map for the optimization of its hot-workability. The map is interpreted on the basis of the dynamic materials model [5], which was reviewed recently by Gegel *et al.* [3] and Alexander [6]. Briefly, the model considers the workpiece essentially as a dissipator of power, and its constitutive equation describes the manner in which the power is converted at any instant into two forms (thermal and microstructural) which are not recoverable by the system. At any instant the total power dissipated consists of two complementary parts: a G content representing the temperature rise and a J co-content representing the dissipation through metallurgical processes. The factor that partitions power between G and J is the strain rate sensitivity (m) of flow stress, and the J co-content is given by [5]

$$J = \sigma\dot{\varepsilon}m/(m + 1) \quad (1)$$

where σ is the flow stress and $\dot{\varepsilon}$ is the strain rate. For an ideal linear dissipator, $m = 1$ and $J = J_{max} = \sigma\dot{\varepsilon}/2$.

0022–2461

The efficiency of power dissipation of a non-linear dissipator may be expressed as a dimensionless parameter

$$\eta = J/J_{max} = 2m/(m + 1) \quad (2)$$

The variation of η with temperature and strain rate represents the characteristics of power dissipation through microstructural changes in the workpiece material and constitutes a processing map.

The power dissipation maps are continuum maps, but the domains may be interpreted in terms of specific atomistic processes. This can be done with the help of Raj maps [7]. In hot deformation there are safe and damage mechanisms that occur in different strain rate–temperature regimes. For example, the safe mechanisms involve dynamic recovery and dynamic recrystallization, whereas damage mechanisms are wedge cracking (which dominates at the lower strain rates and higher temperatures) and void formation at hard particles (which dominates at higher strain rates and lower temperatures). The damage processes are generally highly efficient in dissipating energy through the production of new surfaces, whereas the safe processes are relatively less efficient since power dissipation occurs by annihilation of dislocations or their groups. In the safe regime dynamic recrystallization is more efficient than dynamic recovery. The major advantage of the model is that it helps to establish the material behaviour under "dynamic" conditions, since the efficiency parameter represents the instantaneous power dissipation characteristics.

In this study the hot deformation behaviour of the composite material was evaluated in both the as-sintered powder metallurgy billet stage and the extruded condition. This would help in optimizing the process parameters for both billet conditioning and secondary metal-working steps.

2. Experimental procedure

Ultrasonically gas-atomized commercial-purity 1100 Al powder was blended with 10 vol % SiC_p and compacted using cold isostatic pressing. The billets thus prepared were then sintered under vacuum. One of the billets was canned for further extrusion, whereas the other was utilized for machining cylindrical compression specimens 10 mm in diameter and 15 mm high for hot compression testing in the temperature range 300–550 °C and strain rate range 0.0001–0.1 s^{-1}. The canned billet was extruded at 500 °C using a ram speed of 3 mm s^{-1} and an extrusion ratio of 10 : 1 to produce a rod about 16 mm in diameter. Cylindrical specimens of the above dimensions were machined from the extruded rod for a separate set of hot compression experiments in the temperature range 300–550 °C and strain rate range 0.001–1 s^{-1}. Concentric grooves about 0.5 mm deep were engraved on the specimen faces to facilitate the retention of the lubricant. A 1 mm 45° chamfer was given to the edges of the faces to avoid fold over in the initial stages of the compression. A 0.5 mm diameter hole was drilled to a depth of 5 mm at half the height of each specimen for the insertion of a thermocouple to measure the exact temperature of the specimen during testing. A computer-controlled servohydraulic machine (Dartec, Stourbridge, West Midlands, UK), which had the facility for an exponential decay of actuator speed to give constant true strain rates during testing, was used for the compression testing. In arriving at the exponential decay equation for the stroke–time variation, the small elastic deflections of the machine and the grips were neglected. The temperature control was within ± 2 °C and the adiabatic temperature rise during compression was measured with a thermocouple embedded in the specimen.

The deformed specimens were sectioned parallel to the compression axis and the surface was prepared for metallographic examination using standard metallographic techniques. The polished specimens were etched with an etchant containing 50 ml Poultan's reagent (12HCl, $6HNO_3$, 1HF 48% and $1H_2O$), 25 ml HNO_3 and 40 ml H_2O containing 12 g CrO_3, which was applied for different times depending on the deformation conditions [8]. For the purpose of revealing the grains for grain size measurements, electrolytic polishing and etching was employed. The electrolyte consisted of 25 ml perchloric acid, 40 ml glycerol and 135 ml methanol. Transmission electron microscopy (TEM) studies were also performed on some of the specimens and electrolytic thinning was employed to prepare the thin foils. The tensile properties of the extruded MMC were measured on round specimens with a gauge length of about 27 mm and a diameter of 4 mm.

3. Results

The microstructures of the MMC in the as-sintered and in the as-extruded condition are shown in Figs 1 and 2, respectively. The as-sintered microstructure (Fig. 1) exhibited prior particle boundaries (PPB; average particle size 50 μm) and a uniform distribution of SiC_p. The as-extruded microstructure had an equiaxed grain structure with an average grain diameter of 12 μm, which was much smaller than the prior particle size.

Typical true stress–true plastic strain curves for the MMC in the as-sintered condition recorded at 500 °C and different strain rates are shown in Fig. 3. All

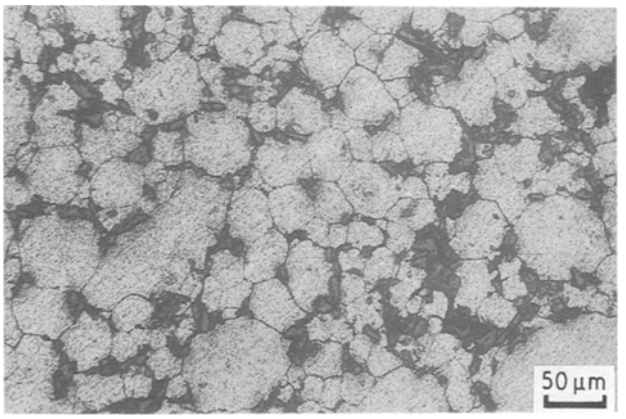

Figure 1 Initial microstructure of 1100 Al–10 vol % SiC (as-sintered).

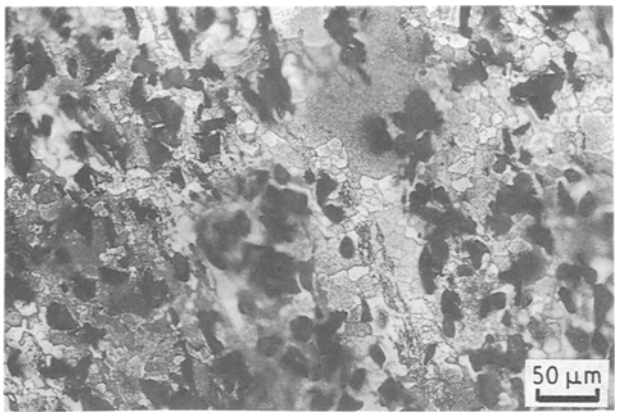

Figure 2 Initial microstructure of 1100 Al–10 vol % SiC (as-extruded).

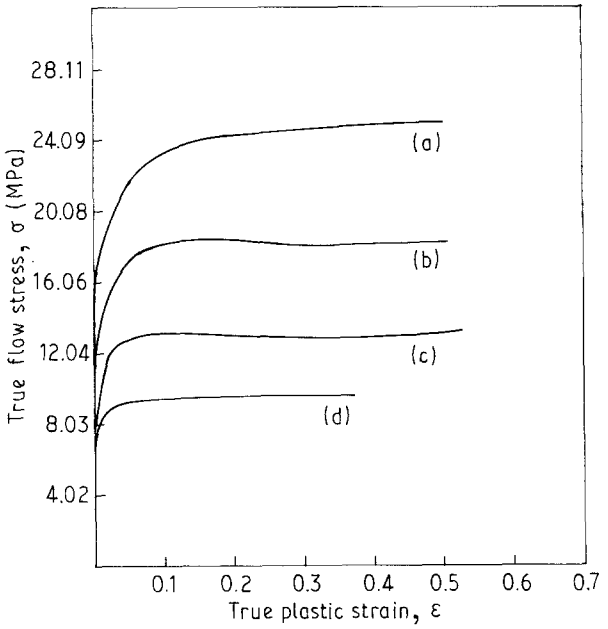

Figure 3 Flow curves for 1100 Al– 10 vol % SiC (as-sintered) at 500 °C and strain rates of (a) 0.1, (b) 0.01, (c) 0.001 and (d) 0.0001.

curves exhibited a steady-state flow behaviour except for those for 300 °C, which showed slight work hardening. The values of flow stress (σ) as a function of temperature (T) and strain rate ($\dot{\varepsilon}$) at a strain (ε) of 0.3 for the MMC are shown in Table I.

TABLE I Values of flow stress (in MPa) of 1100 Al–10 vol % SiC in both as-sintered and as-extruded conditions at different temperatures and strain rates at a strain of 0.3

Strain rate (s^{-1})	Temperature (°C)					
	300	350	400	450	500	550
As-sintered condition						
0.0001	36.0	23.3	17.4	12.3	8.8	8.3
0.001	41.3	28.6	18.6	15.6	11.8	9.1
0.01	54.0	35.0	22.4	22.4	16.7	12.7
0.1	61.9	40.8	28.6	31.7	22.5	17.7
As-extruded condition						
0.001	32.0	26.1	20.7	17.2	14.0	10.5
0.01	43.9	34.1	26.1	22.0	18.4	13.5
0.1	59.8	42.9	35.1	27.9	22.9	18.8
1.0	82.5	61.5	47.8	37.5	31.0	23.0

Power dissipation maps were constructed using the above data and the principles of dynamic materials modelling [3, 5, 6]. The map software adopted the following procedure: log (flow stress) versus log (strain rate) data at a constant temperature and strain were fitted using a cubic spline function, and m was calculated as a function of the strain rate. This was repeated at different temperatures. The efficiency of power dissipation through microstructural changes [$\eta = 2m/(m + 1)$] was then calculated from a set of m-values as a function of the strain rate and temperature, and was plotted as a three-dimensional map. The three-dimensional variation is better viewed as an iso-efficiency contour map in the strain rate–temperature plane. The power dissipation map for the MMC in the as-sintered condition at a strain of 0.3 is shown in Fig. 4a in three dimensions and in Fig. 4b as a contour map where η is plotted as a percentage. The maps obtained at other strains are essentially identical to that in Fig. 4. The map exhibits two different domains: first, a domain centred at 500 °C and 0.01 s^{-1} with a peak efficiency of about 30% and, secondly, a domain centred at about 300 °C and 0.001 s^{-1} with a peak efficiency of about 21%.

The mechanical properties of the MMC in the as-extruded state are given in Table II. Typical true stress–true plastic strain curves for the MMC in the as-extruded state recorded at 450 °C and different strain rates are shown in Fig. 5. The curves at other temperatures were similar to these and show slight flow softening at higher strain rates (1.0 s^{-1}) and nearly steady-state flow behaviour at lower strain rates. The values of σ as a function of T, $\dot{\varepsilon}$ and ε for the MMC in the as-extruded condition are shown in Table I. Power dissipation maps were constructed using the above data, and the map at a strain of 0.3 is shown in Fig. 6a in three dimensions and in Fig. 6b as a contour map. The maps obtained at other strains were very similar to that at 0.3 strain. The map exhibits one major domain centred at 425 °C and 1 s^{-1} with a peak efficiency of about 30%. There are other minor domains with lower efficiencies (< 25%) occurring at about 300 °C and 0.001 s^{-1} (η = 25%), at 475 °C and 0.001 s^{-1} (η = 23%) and at 550 °C and 0.01 s^{-1} (η = 24%).

A comparison of this map (Fig. 6b) with that for the MMC in the as-sintered condition (Fig. 4b) reveals the following differences. First, the domain of the map for the MMC in the as-sintered condition occurring at 500 °C and 0.01 s^{-1} shifted to a lower temperature (425 °C) and higher strain rate (1 s^{-1}) in the map for the MMC in the extruded condition. Secondly, the domain of the map for the MMC in the as-sintered condition occurring at 300 °C and 0.001 s^{-1} remained unchanged except for a slight increase in the peak efficiency value from 20 to 25%. Finally, two more minor domains with efficiencies < 25% appeared in the map for the MMC in the extruded condition.

4. Discussion

4.1. Interpretation of power dissipation maps

The basis for the interpretation of the power dissipation maps is the dynamic materials model [3, 5, 6]

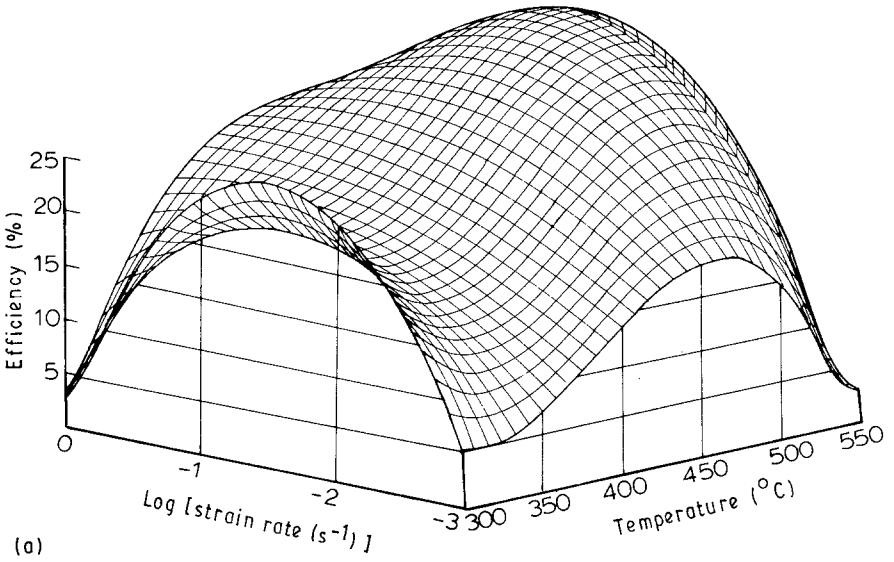

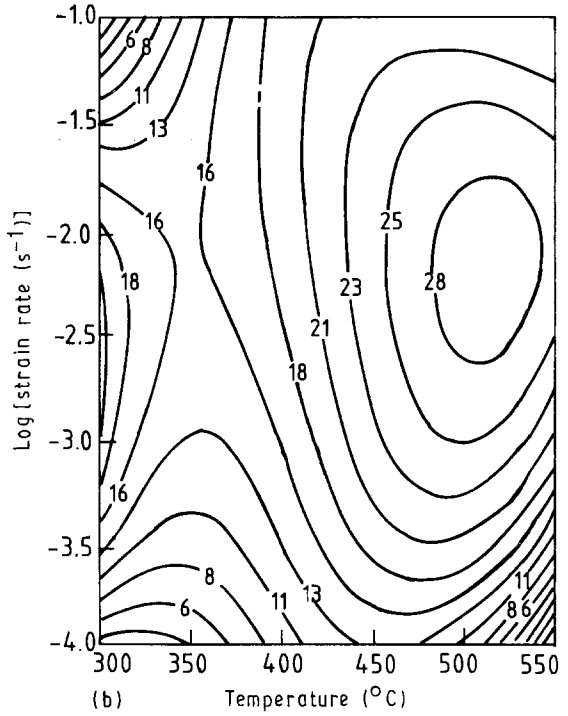

Figure 4 Processing maps (a) in three dimensions and (b) in two dimensions for 1100 Al–10 vol % SiC (as-sintered) at a strain of 0.3.

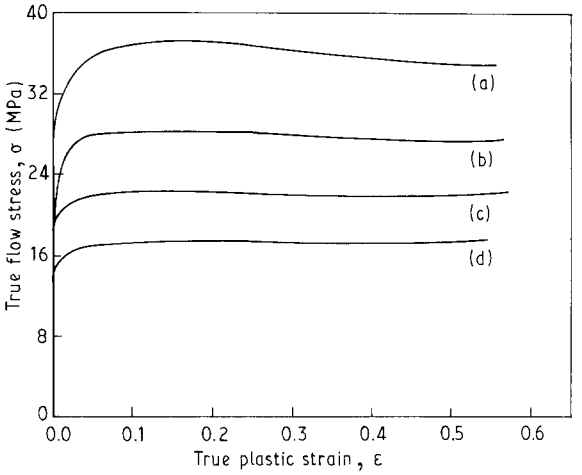

Figure 5 Flow curves for 1100 Al–10 vol % SiC (as-extruded) at 450 °C and strain rates of (a) 1.0, (b) 0.1, (c) 0.01 and (d) 0.001.

TABLE II Tensile properties of Al–10 vol % SiC extruded composite

Yield strength (MPa)	Ultimate tensile strength (MPa)	Young's modulus (GPa)	Elongation (%)
75	114	96	20

described above. The maps are interpreted on the basis of the atomistic approach of Raj [7]. The domain occurring at 500 °C and 0.01 s^{-1} in MMCs (Fig. 4b) in the as-sintered condition has a peak efficiency of about 30% and represents the process of DRX since this process occurs at intermediate strain rates and higher temperatures. The microstructure of the MMC deformed at the peak of the domain (500 °C and 0.01 s^{-1}) is shown in Fig. 7. In comparison with the initial microstructure (Fig. 1) the DRX microstructure exhibited considerable reconstitution in terms of grain size and shape. A closer examination of the microstructure obtained at the DRX peak (Fig. 8) has shown that smaller nuclei of DRX are present at the grain boundaries, which are themselves corrugated or wavy. These observations clearly confirm that the domain represents DRX of the matrix in the MMC. In the DRX structure shown in Fig. 7 a new equiaxed set of grains could be seen, and this suggests that a reconstitution of the original prior particle boundary structure had occurred.

The domain occurring at 300 °C and 0.001 s^{-1} in the map for the as-sintered MMC was characterized by a lower efficiency (21%) and therefore represents dynamic recovery of the matrix. The microstructure of the specimen deformed under these conditions is shown in Fig. 9. The microstructure was characterized by a very fine grain size caused by static recrystallization occurring during cooling following dynamic recovery. The stress–strain curves at the lower temperature showed slight hardening typical of dynamic recovery. A similar domain occurring at 300 °C and 0.001 s^{-1} in the map for the as-extruded MMC also represents the process of dynamic recovery.

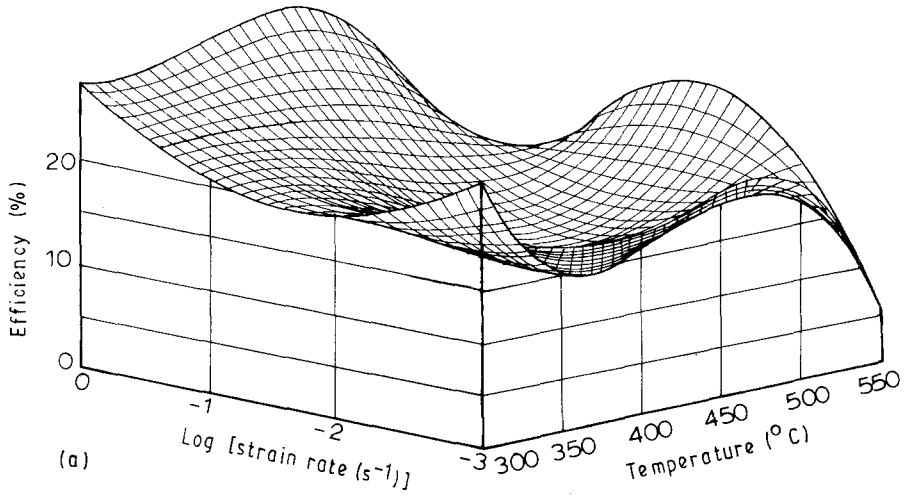

Figure 6 Processing maps (a) in three dimensions and (b) in two dimensions for 1100 Al–10 vol % SiC (as-extruded) at a strain of 0.3.

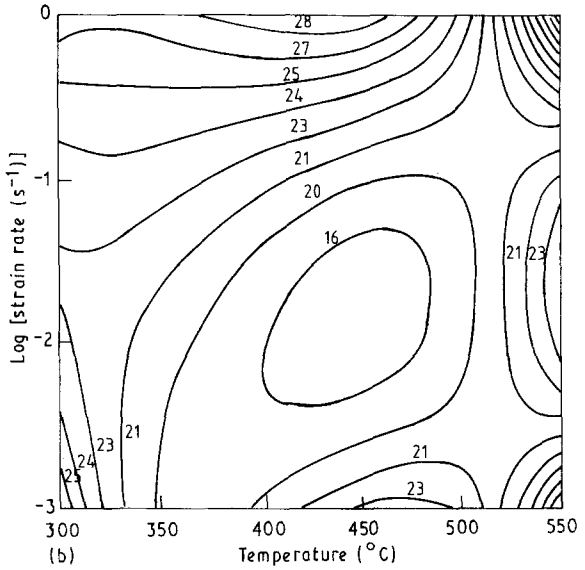

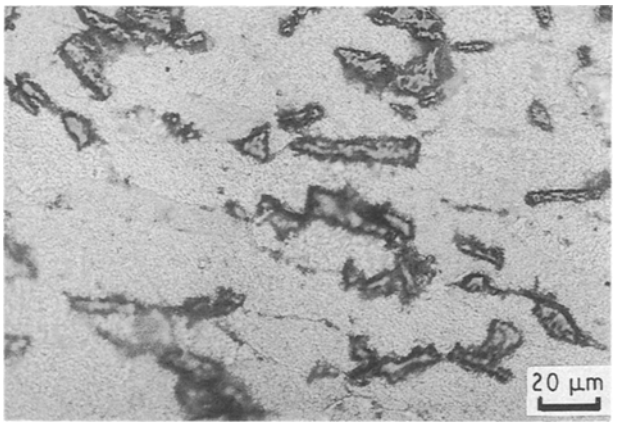

Figure 8 Microstructure of the MMC (as-sintered) deformed at 500 °C and 0.01 s^{-1} at a higher magnification than in Fig. 7.

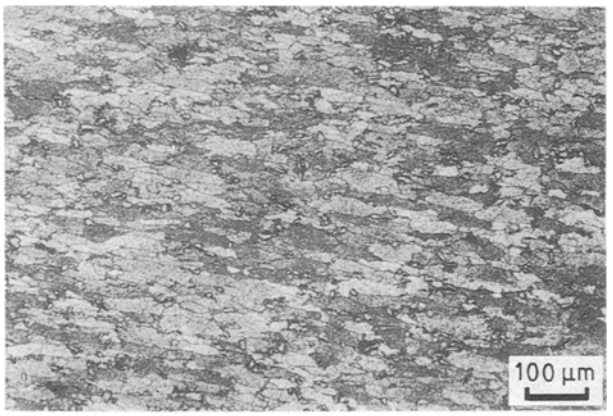

Figure 7 Microstructure of the MMC (as-sintered) deformed at 500 °C and 0.01 s^{-1}.

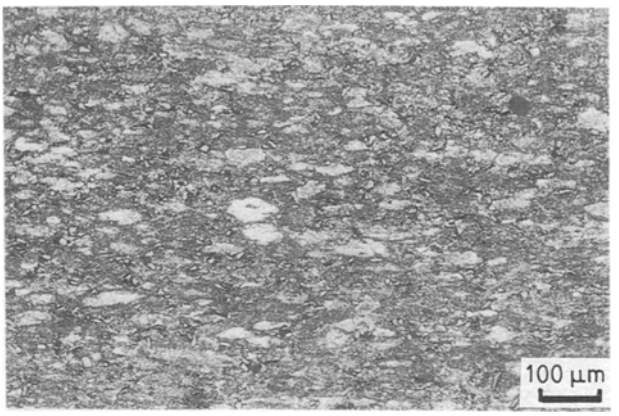

Figure 9 Microstructure of the MMC (as-sintered) deformed at 300 °C and 0.001 s^{-1}.

The domain occurring at 350–450 °C and 1 s^{-1} in the MMC in the as-extruded condition (Fig. 6b) also represents the DRX domain. The DRX microstructure corresponding to the specimen deformed at these temperature and strain rates (450 °C and 1 s^{-1}) is shown in Fig. 10. This again shows a major reconstitution of the microstructure of the as-extruded MMC to produce a completely recrystallized equiaxed grain structure. The measured variation in the recrystallized grain size with temperature in the DRX domain is shown in Fig. 11 and compared with the efficiency variations. The grain size variation with temperature was sigmoidal and similar to that generally observed in static recrystallization. Following the convention

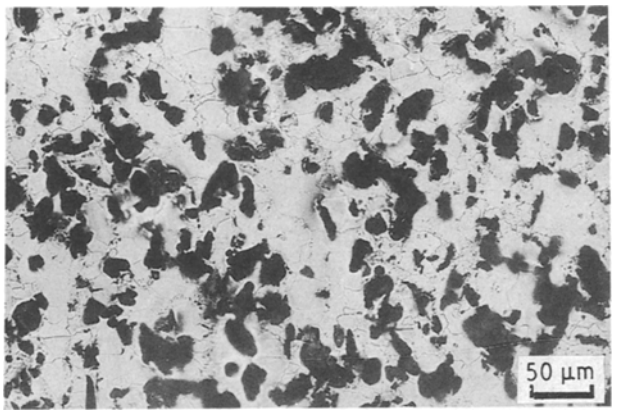

Figure 10 Microstructure of the MMC (as-extruded) deformed at 450 °C and 1 s^{-1}.

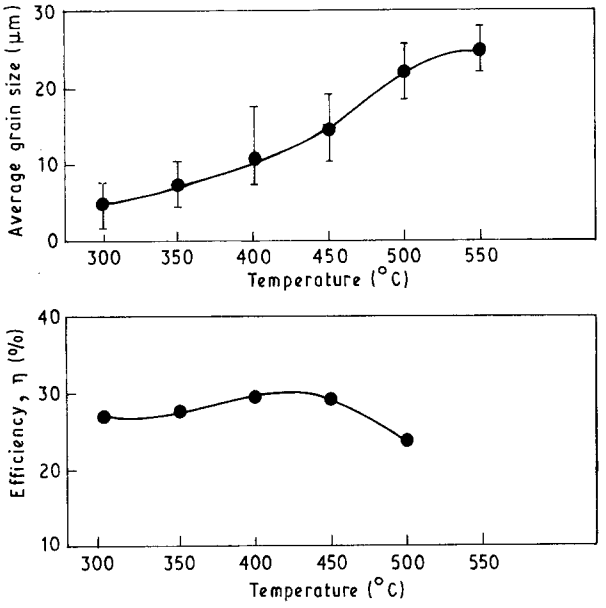

Figure 11 Grain size and efficiency variation as a function of temperature for the MMC (as-extruded) deformed at 1 s^{-1}.

used for static recrystallization, the temperature corresponding to a 50% change in the grain size represents the DRX temperature, which also coincides with the temperature for the peak efficiency (425 °C). It is interesting to note that in the as-extruded MMC the DRX domain shifted to lower temperatures and higher strain rates than that in the as-sintered MMC, whereas the peak efficiency of power dissipation remained unchanged. DRX involves migration of grain boundaries as a critical step [9], and the distance of migration in the case of as-sintered materials is limited to the prior particle size in the matrix. Upon extrusion, the prior particle undergoes dynamic recrystallization (Fig. 2) and hence the grain size within the particle is smaller. The distance of migration is therefore reduced and the boundary takes a shorter time to cover the distance, thereby increasing the strain rate for DRX. Furthermore, in extruded materials a fine dislocation substructure forms upon hot deformation, leading to subgrain formation (Fig. 12). As the driving force for the migration of boundaries during high-temperature deformation is the reduction of the total interface energy, the fine subgrain structure enhances the rate of

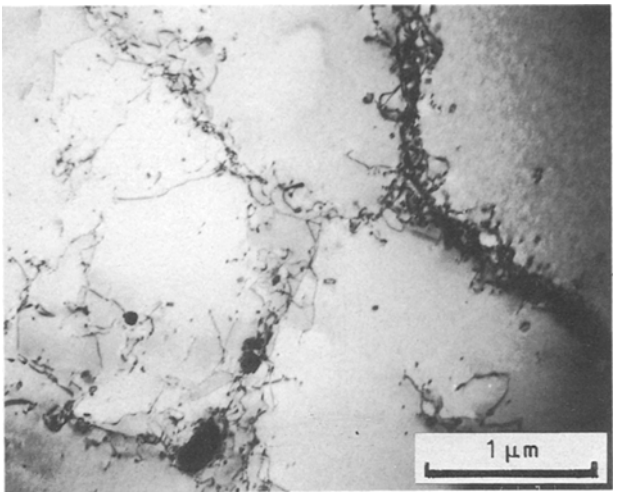

Figure 12 Fine dislocation cell structure in the extruded MMC which leads to subgrain formation as revealed by TEM.

migration, and therefore the strain rate for DRX is high. This large driving force is also responsible for the reduction in the DRX temperature in the as-extruded MMC.

At high temperatures and high strain rates the MMC in the extruded condition exhibited extensive cracking. A typical microstructure of the specimen deformed at 550 °C and 1 s^{-1} is shown in Fig. 13. This regime of cracking should be strictly avoided in processing. The other minor domains at 475 °C and 0.001 s^{-1} and at 550 °C and 0.01 s^{-1} in the map for the as-extruded MMC are not fully developed, and hence cannot be interpreted with any certainty.

4.2. Implications in the optimization of processing

The as-sintered MMC powder compacts have prior particle boundary defects which must be eliminated by hot-working in order to improve the workability. For this purpose processing in the dynamic recrystallization regime is preferred, since DRX reconstitutes the microstructure and redistributes the prior particle boundary defects. Thus, billet conditioning of the as-sintered compacts of the MMC is best done at 500 °C

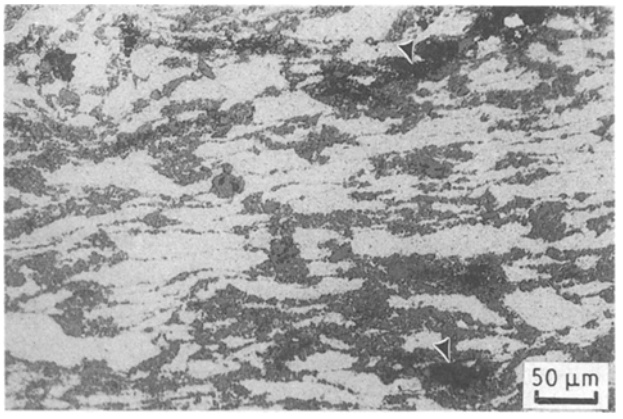

Figure 13 Microstructure of the MMC (as-extruded) deformed at 550 °C and 1 s^{-1} showing large cracks (arrows).

and 1 s^{-1}, which are the optimum parameters for DRX. The extrusion was carried out successfully using these parameters and the extruded stock had good mechanical properties (Table II). On the other hand, secondary metal-working operations involving further processing such as forging after extrusion may be done at higher strain rates (1 s^{-1}) and lower temperatures (425 °C) as the DRX domain in the as-extruded MMC becomes shifted in that direction.

5. Conclusions

From the processing maps obtained for the hot-working of 1100 Al–10 vol % SiC_p MMC in the as-sintered as well as extruded conditions, the following conclusions were drawn regarding the flow behaviour of the MMC in the temperature range 300–550 °C.

1. Dynamic recrystallization of the MMC in the as-sintered condition occurs at 500 °C and 0.01 s^{-1} strain rate, and has an efficiency of about 30%. The microstructure in this domain exhibited a reconstitution of the prior microstructure.

2. The DRX strain rate for the MMC in the extruded condition is higher (1 s^{-1}) than that for the as-sintered condition (0.01 s^{-1}), whereas the DRX temperature is lower (425 °C).

3. The results are explained in terms of the enhanced grain boundary migration in the MMC, caused by the fine subgrain structures which are produced as a result of the high rate of dislocation generation.

4. At 300 °C and a strain rate of 0.001 s^{-1} both the as-sintered and the extruded MMC exhibited a dynamic recovery domain with a peak efficiency of 21%.

5. The MMC exhibited cracking when deformed at 550 °C and 1 s^{-1} strain rate, and these conditions should be avoided in the processing of the MMC.

6. It is recommended that billet conditioning by extrusion of the MMC in the as-sintered condition be done at 500 °C and 0.01 s^{-1}, whereas secondary metal-working may be conducted at higher strain rates (1 s^{-1}) and lower temperatures (425 °C).

Acknowledgements

The authors thank Dr Dipanker Banerjee, Associate Director, DMRL, Hyderabad, for permitting the publication of this work. Mr V. V. Bhanuprasad, Scientist, DMRL, is gratefully acknowledged for his help in producing the MMC. One of the authors (Y.V.R.K.P.) is grateful to Dr H. L. Gegel, formerly of WPAFB, Ohio, USA, and now with Universal Energy Systems, Dayton, Ohio, USA, for introducing him to this area of research and for many inspiring discussions.

References

1. A. D. DIVECHA, S. G. FISHMAN and S. D. KARMARKAR, *J. Metals* **33** (1981) 12.
2. S. V. NAIR, J. K. TIEN and R. C. BATES, *Int. Met. Rev.* **30** (1985) 275.
3. H. L. GEGEL, J. C. MALAS, S. M. DORAIVELU and V. A. SHENDE, in "Metals Hand Book", Vol. 14 (American Society of Metals, Metals Park, Ohio, 1987) p. 417.
4. F. R. TULER and T. F. KLIMOWICZ, in "Metal and Ceramic Matrix Composites; Processing, Modelling and Mechanical Behaviour" (The Minerals, Metals and Materials Society, Warrendale, Pa, 1990) p. 271.
5. Y. V. R. K. PRASAD, H. L. GEGEL, S. M. DORAIVELU, J. C. MALAS, J. T. MORGAN, K. A. LARK and D. R. BARKER, *Met. Trans.* **15A** (1984) 1883.
6. J. M. ALEXANDER, in "Modelling Hot Deformation of Steels – An Approach to Understanding and Behaviour" (Springer-Verlag, Berlin, 1989) p. 101.
7. R. RAJ, *Met. Trans.* **12A** (1981) 1089.
8. H. J. McQUEEN, E. EVANGELISTA, J. BOWLES and G. CRAWFORD, *Met. Sci.* **18** (1984) 395.
9. N. RAVICHANDRAN and Y. V. R. K. PRASAD, *Bull. Mater. Sci.* **14** (1991) 1241.

Received 19 November 1991
and accepted 2 September 1992